energies

Article

Modeling and Analysis of Low-Frequency Oscillation for Electrified Railway under Mixed Operation of Passenger and Freight Trains

Yunling Wang [1], Ting Li [1], Jiawei Liu [1], Fang Liu [1], Yunche Su [1], Qiao Zhang [2,*], Weilu Zhang [2] and Zhigang Liu [2]

1 State Grid Sichuan Economic Research Institute, Chengdu 610041, China
2 School of Electrical Engineering, Southwest Jiaotong University, Chengdu 610032, China
* Correspondence: zhangqiao_jq@163.com; Tel.: +86-028-87600213

Abstract: Addressing the shortcomings of existing low-frequency oscillation research on electrified railways, which has mainly focused on single-type trains and lacks the accurate modeling of traction inverter systems, in this paper we modeled and analyzed low-frequency oscillations in an electrified railway passenger and freight mixed-operation vehicle–grid system. First, an equivalent model of the DC side of the traction inverter was established, with the inverter system being equivalent to the parallel connection of the load resistance and the current source, and the specific mathematical expression was determined and verified by impedance measurement. Secondly, based on the equivalent model of the DC side of the traction inverter, a small signal model of the vehicle–grid system under the mixed operating conditions of CRH5 and HXD_{2B} considering the inverter system was established. The generalized Nyqusit criterion was used to study the low-frequency oscillation characteristics under mixed transportation conditions. The accuracy of the established model and the correctness of the theoretical analysis were verified based on Matlab/Simulink. Finally, using the dominant pole theory to analyze the low-frequency stability conditions, the relationship between the number of mixed trains and the minimum short-circuit ratio was obtained, and the simulation verification was carried out.

Keywords: electrified railway; low-frequency oscillation; traction inverter system; mixed operation

check for updates

Citation: Wang, Y.; Li, T.; Liu, J.; Liu, F.; Su, Y.; Zhang, Q.; Zhang, W.; Liu, Z. Modeling and Analysis of Low-Frequency Oscillation for Electrified Railway under Mixed Operation of Passenger and Freight Trains. *Energies* **2022**, *15*, 7544. https://doi.org/10.3390/en15207544

Academic Editors: Ahmed Abu-Siada and Nicu Bizon

Received: 6 September 2022
Accepted: 10 October 2022
Published: 13 October 2022

1. Introduction

At present, the EMUs put into operation in China generally adopt the AC–DC–AC traction drive mode. With the promotion of electrified railways under the support of national policies, more and more electric locomotives have been put into use. This also means that more power electronics devices with nonlinear characteristics are connected to the TN, which leads to frequent LFO and harmonic instability problems in the "multi-vehicle–grid-connected" system, which brings a great threat to the VGS [1,2]. The trains currently in operation are mainly passenger trains represented by CRH and freight locomotives represented by HXD. Although these two types of trains represent AC–DC–AC loads, their grid-side converters mainly adopt two different control strategies, namely DQDC and TDCC. Studies have shown that when two trains with different control structures are put into operation at the same time, their control parameters affect not only their impedance characteristics but also the stability of other vehicles. Therefore, the LFO mechanism of the VGS under different mixed running conditions is more complicated [3].

Generally speaking, research on LFO has mainly been carried out from two perspectives: mechanism analysis and measures for suppressing LFO. In the study of the LFO problem, the frequency domain impedance method is widely adopted, that is, the VGS is regarded as the cascade of the TN subsystem and the train subsystem [4,5]; the impedance models of the two subsystems are established separately; and the impedance ratio matrix is further obtained to analyze the system stability [6–8]. Since LFO usually occurs in low-power conditions when multiple trains are hoisted at the same location, the single-phase grid-side converter is mainly considered when establishing the train impedance model [9]. The research shows that the LFO phenomenon is mainly caused by the mismatch between the parameters of the TN system and the controller parameters of the EMUs [10]. In [10], the impedance model was used to draw a Nyquist curve and a Bode diagram, which better reflected the dynamic interaction influence at the common connection points of the VGS and clearly reflected the frequency band of the unstable region. However, this paper only analyzed the current control of the locomotive and lacked an analysis of the entire locomotive control system. The dq decoupling small-signal impedance model of CRH5 EMUs was established in [11,12], and the influence of the number of single CRH5 EMUs and the load and control parameters on the LFO of the VGS was analyzed. The authors of [13] established the locomotive harmonic state space (HSS) model and analyzed the harmonic stability of the VGS. Since the HSS model contains multiple cross-coupled dynamics and harmonic components of electricity, the derived model can accurately evaluate the LFO problem of the VGS. In [14], the difference and applicability of the harmonic linearization method and the HSS method were explained according to the harmonic characteristics of the DC converter. The authors of [15,16] took the CRH3 as an example and analyzed the influence of the number of trains and the control parameters on the low-frequency stability, but the conclusions lacked a mechanism explanation. The authors of [17] proposed an analysis method to judge the stability according to the open-loop pole, but compared with the generalized Nyquist criterion [10], these methods have greater limitations in analyzing the stability of the system. The authors of [5,6] established a small-signal impedance model of a single rectifier based on the impedance analysis method and combined the generalized Nyquist criterion and the dominant pole to analyze the influence of the proportional parameters of the voltage and current loop on the stability of the VGS. The authors of [18] established a single-phase dq decoupling small-signal impedance model for CRH5 EMUs and used the dominant pole to analyze the influence of the external parameters of the VGS and the internal control parameters on the LFO.

Most studies on LFO in the above-mentioned literature were carried out under the operating conditions of a single-control-type train, and the mechanism of the occurrence of LFO was considered in terms of impedance. Few authors have considered the LFO phenomenon of the VGS when different types of trains are mixed. In [19,20], different kinds of locomotives were simulated under mixed running conditions, and the grid-side current and voltage harmonics before and after mixed running were analyzed. However, the mechanism of the influence of various parameters on the low-frequency stability was not analyzed. In addition, the existing literature has not considered the structure of the inverter and traction motor when modeling the vehicle-side impedance, and the inverter and the traction motor have been replaced by the load resistance. To address the above problems, in this paper we studied the LFO of the passenger and freight mixed-operation VGS of electrified railways. The main aims and innovations were as follows.

(1) In this paper, a DC-side equivalent model of the traction inverter was first established, with the inverter system being equivalent to the parallel connection of the load resistance and the current source, and the specific mathematical expression was determined and verified by impedance measurement.
(2) Based on the DC-side equivalent model of the traction inverter, a small-signal model of the VGS under the mixed operating conditions of CRH5 and HXD_{2B} considering the inverter system was established. The generalized Nyqusit criterion was used to study the LFO characteristics of the VGS under mixed transportation conditions, and the validity of the established model and the correctness of the theoretical analysis were verified through a time-domain simulation using Matlab/Simulink.
(3) Using the dominant pole theory to analyze the low-frequency stability conditions of the VGS, the relationship between the number of mixed trains and the minimum

short-circuit ratio of the system was obtained, and the simulation verification was carried out.

2. Impedance Model of VGS under Mixed Operation of Passenger and Freight Locomotives

This paper takes the CRH5 EMUs and the HXD_{2B} locomotive as the study object to investigate mixed operation. The CRH5 rectifier adopts the DQDC method, and the HXD_{2B} rectifier adopts the TDCC control method. A schematic diagram of the mixed operation is shown in Figure 1. A corresponding control block diagram is shown in Figure 2. The control strategy of DQDC takes the detected single-phase AC voltage and current as the α system and constructs the β system component through the SOGI. After the PLL locks the phase of the grid voltage, the voltage and current under the $\alpha\beta$ system are converted to the dq system by the Park transformation, which is controlled by the controller. The control structure of an outer voltage loop and inner current loop is adopted. Finally, the obtained control signal under the dq system is subjected to inverse Park transformation, and the control signal under the α system is taken to send out PWM waves to control the main circuit. The control strategy of TDCC is to orthogonalize the detected single-phase AC voltage through the SOGI-PLL. The introduction of feedforward in the DC voltage control loop improves the dynamic response of the PI controller. The reference current amplitude obtained by the DC voltage loop and the grid voltage phase locked by PLL are input into the current control loop to realize the phase synchronization of the current. The reference modulation signal is obtained from the current loop to control the main circuit. As shown in Figure 2, the SOGI-PLL takes the input voltage and inductor current e_n and i_n as α-system components and obtains imaginary β-system components under the action of SOGI. The semaphore under the $\alpha\beta$ system is decomposed into the dq system through Park transformation. The voltage and current under the dq system are used as control variables to control the system under the action of the controller. The phase angle required for the coordinate transformation is provided by the PLL.

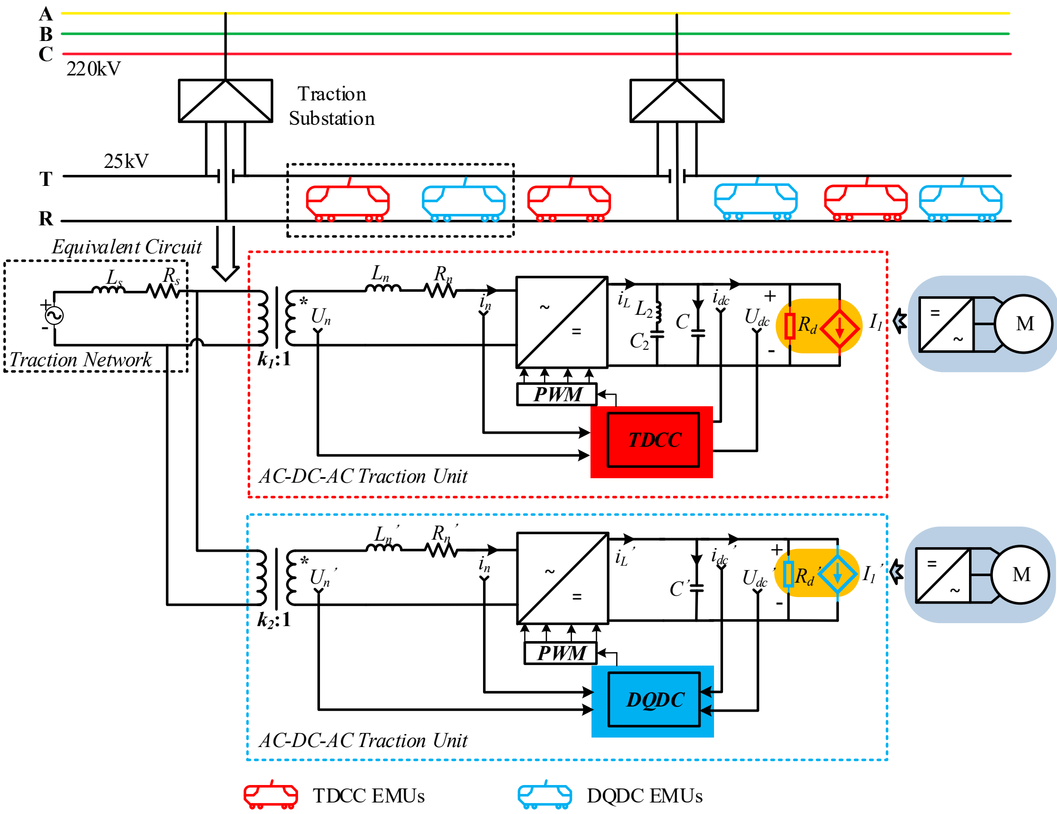

Figure 1. Schematic diagram of mixed operation of passenger and freight locomotives.

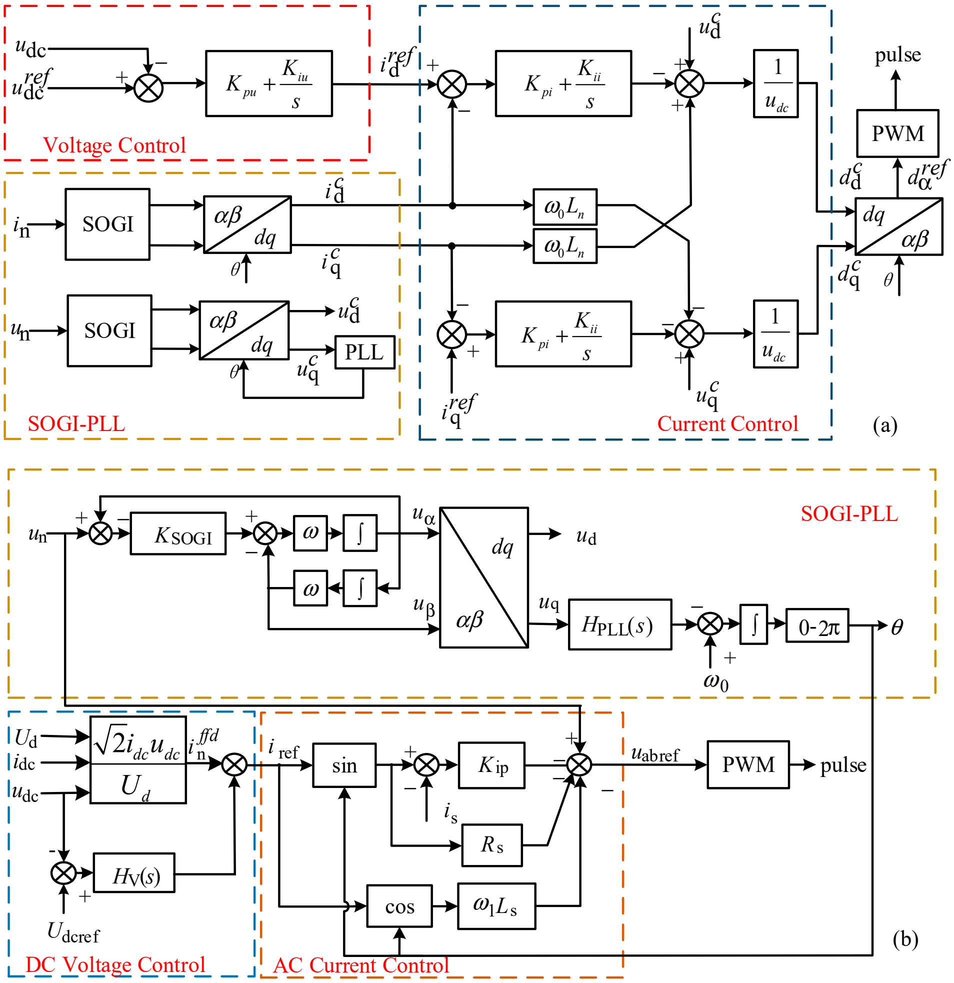

Figure 2. (**a**) Control structure of the rectifier in CRH5. (**b**) Control structure of the rectifier in HXD_{2B}.

When studying the LFO problem, the distributed capacitance of the TN can be ignored. The TN is equivalent to a series circuit containing resistance and inductance. The train consists of several traction drive units in parallel. The traction drive unit contains on-board transformers, grid-side rectifiers, intermediate DC links, traction inverters, and traction AC motors. In this section, the inverter and traction motor are modeled as resistors and current sources in parallel. Then, a unified impedance model considering the inverter for these two types of models is established in the dq coordinate system, which provides a basis for the subsequent theoretical analysis of stability. This paper will study a HXD_{2B} electric locomotive with a TDCC grid-side converter and a CRH5 train with a DQDC grid-side converter. The main circuit and control parameters are shown in Table 1 [12,21].

Table 1. Parameters of VGS.

Parameter	CRH5	HXD_{2B}	Parameter	CRH5	HXD_{2B}
E_d	1770 V	2100 V	K_{iSOGI}	1	1
f_1	50 Hz	50 Hz	K_{Ppll}	0.7	0.7
f_p	[1, 125] Hz	[1, 125] Hz	K_{Ipll}	25	25
R_n	0.145 Ω	0.15 Ω	K_{Pi}	2	0.2
L_n	5.4 mH	4 mH	K_{Ii}	50	0
C_d	9 mF	9 mF	K_{Pu}	0.5	0.3
U_{dc}	3600 V	3750 V	K_{Iu}	5	15
K_{uSOGI}	1	1	f_s	250 Hz	800 Hz

2.1. Equivalent Model of TN

In the low-frequency range, the distributed capacitance of the TN is negligible. Therefore, this paper simplifies the TN as the series connection of resistance and inductance, and its dq small-signal impedance model is shown in (1).

$$\boldsymbol{Z_o} = \begin{bmatrix} R_s + sL_s & -\omega_1 L_s \\ \omega_1 L_s & R_s + sL_s \end{bmatrix} \tag{1}$$

where R_s and L_s represent the grid-side equivalent resistance and equivalent inductance of the traction power supply system, respectively, and ω_1 is the fundamental angular frequency.

2.2. Equivalent Model of Traction Inverter System

At present, the electric locomotives running on electrified railways are generally AC–DC–AC traction drive systems, which are mainly composed of onboard transformers, four-quadrant rectifiers, intermediate DC links, inverters, and traction motors [22,23]. In the AC–DC–AC variable-frequency speed regulation system, the AC side of the PWM inverter can always be equivalent to the three-phase AC electromotive force and the resistance–inductance series circuit [24]. LFO usually occurs in low-power conditions when multiple trains are hoisted and prepared at the same location. At this time, the rectifier and inverter are energized and start to work, and the motor also begins to be energized, but it does not yet rotate. This state can be regarded as a motor stall or short-circuit state, and the induced electromotive force of the motor can be ignored. Therefore, the motor can be equivalent to the form of a resistance–inductance series circuit. The equivalent circuit model of the two-level traction inverter is shown in Figure 3. In this figure, $u_{\rm dc}$ represents the DC-side voltage; $i_{\rm dc}$ represents the DC-side current; u_k (k = 1, 2, 3) represents the instantaneous value of the inverter's three-phase voltage; $R_{\rm e}$ represents the total equivalent resistance of each phase of the traction motor; and $L_{\rm e}$ represents the total equivalent inductance of each phase of the traction motor.

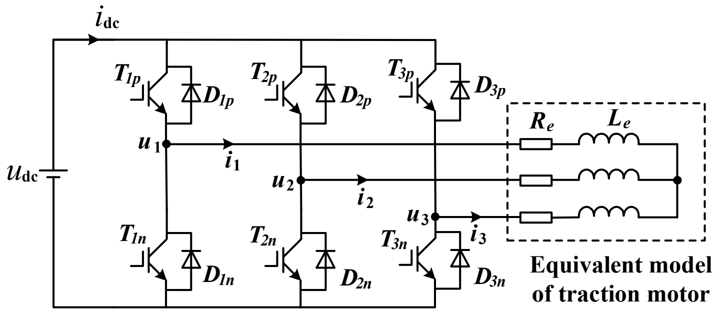

Figure 3. Equivalent model of the two-level traction inverter system.

According to Figure 3, the state space average model of the three-phase inverter circuit can be obtained as shown in (2) [24].

$$\begin{bmatrix} L_{\rm e}\frac{{\rm d}i_1}{{\rm d}t} \\ L_{\rm e}\frac{{\rm d}i_2}{{\rm d}t} \\ L_{\rm e}\frac{{\rm d}i_3}{{\rm d}t} \end{bmatrix} = \begin{bmatrix} -R_{\rm e} & 0 & 0 \\ 0 & -R_{\rm e} & 0 \\ 0 & 0 & -R_{\rm e} \end{bmatrix} \begin{bmatrix} i_1 \\ i_2 \\ i_3 \end{bmatrix} - \begin{bmatrix} (d_{\rm M} - d_1)u_{\rm dc} \\ (d_{\rm M} - d_2)u_{\rm dc} \\ (d_{\rm M} - d_3)u_{\rm dc} \end{bmatrix} \tag{2}$$

In (2), i_k (k = 1, 2, 3) represents the instantaneous value of the three-phase current; d_1, d_2, and d_3 are the duty cycles of the switches on the upper arms of the three-phase half-bridge; and $d_{\rm M}$ is the average value of the three-phase duty cycles.

Expanding and recombining the matrix in (2), (3) can be obtained.

$$L_{\rm e}\, \dot{i}_k + i_k R_{\rm e} = (d_k - d_{\rm M})u_{\rm dc} \tag{3}$$

where

$$d_{\mathrm{M}} = \frac{1}{3}\sum_{k=1}^{3} d_k = \frac{1}{2} \tag{4}$$

In order to obtain the equivalent model of the DC side of the inverter, we solved Formula (3), assuming

$$d_k = \frac{1}{2} + \frac{m}{2}\sin[\omega_{\mathrm{e}}t - (k-1)120^\circ] \tag{5}$$

where m is the modulation coefficient of the PWM inverter, and ω_{e} is the three-phase current frequency of the motor stator. Let $\alpha_k = \omega_{\mathrm{e}}t - (k-1)120^\circ$, then (3) could be rewritten as (6):

$$L_{\mathrm{e}}\dot{i}_k + i_k R_{\mathrm{e}} = \frac{mu_{\mathrm{dc}}}{2}\sin\alpha_k \tag{6}$$

Let

$$\begin{cases} u_k = \frac{mu_{\mathrm{dc}}}{2}\sin\alpha_k \\ U_k = \frac{mu_{\mathrm{dc}}}{2}(k = 1, 2, 3) \end{cases} \tag{7}$$

where U_k represents the three-phase voltage amplitude of the inverter.

Let the steady-state solution of Equation (6) be

$$i_{kp} = I\sin(\alpha_k - \gamma) \tag{8}$$

where I is the amplitude of the three-phase current, and γ is the angle to be solved.

Substituting (8) into (6), the steady-state equation of (6) could be obtained as follows:

$$\omega_{\mathrm{e}}L_{\mathrm{e}}I\cos(\alpha_{\mathrm{k}} - \gamma) + IR_{\mathrm{e}}\sin(\alpha_{\mathrm{k}} - \gamma) = U_{\mathrm{k}}\sin\alpha_{\mathrm{k}} \tag{9}$$

By making further adjustments, we obtained

$$(\omega_{\mathrm{e}}L_{\mathrm{e}}I\cos\gamma - IR_{\mathrm{e}}\sin\gamma)\cos\alpha_k + (IR_{\mathrm{e}}\cos\gamma + \omega_{\mathrm{e}}L_{\mathrm{e}}I\sin\gamma)\sin\alpha_k = U_k\sin\alpha_k \tag{10}$$

From (10), we determined:

$$\begin{cases} \omega_{\mathrm{e}}L_{\mathrm{e}}I\cos\gamma - IR\sin\gamma = 0 \\ \omega_{\mathrm{e}}L_{\mathrm{e}}I\sin\gamma + IR\cos\gamma = U_k \end{cases} \tag{11}$$

Therefore, (12) could be obtained.

$$\begin{cases} I = \sqrt{\frac{U_k^2}{R_{\mathrm{e}}^2 + (\omega_{\mathrm{e}}L_{\mathrm{e}})^2}} \\ \gamma = \arctan\left(\frac{\omega_{\mathrm{e}}L_{\mathrm{e}}}{R_{\mathrm{e}}}\right) \end{cases} \tag{12}$$

Let the full solution to Equation (6) be

$$i_k = A_k e^{-t/\tau} + I\sin(\alpha_k - \gamma) \tag{13}$$

where A_k is the undetermined coefficient, τ is the time constant, and $\tau = L_{\mathrm{e}}/R_{\mathrm{e}}$.

Substituting $i_k(0) = 0$ into Equation (13), the expression of A_k could be obtained as follows:

$$A_k = I\sin[\gamma + (k-1)120^\circ] \tag{14}$$

The DC current and the three-phase stator current satisfy the relationship shown in (15).

$$i_{\mathrm{dc}} = \sum_{k=1}^{3} d_{\mathrm{k}} i_{\mathrm{k}} \tag{15}$$

Substituting (13) and (14) into (15), the expression of i_{dc} could be obtained as follows:

$$i_{\mathrm{dc}} = \frac{3m}{4} I \left[\cos\gamma - \cos(\omega_{\mathrm{e}} t + \gamma) e^{-t/\tau} \right] \tag{16}$$

Since the value of the time constant τ is generally small, after ignoring the transient process, the inverter circuit and the motor could be regarded as equivalent to a parallel connection of a load resistor R_{d} and a current source I_1, as shown in Figure 4.

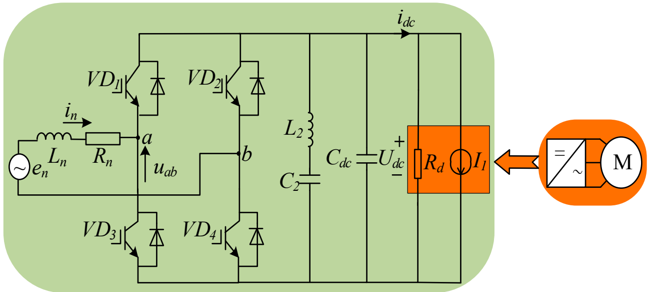

Figure 4. The equivalent schematic diagram of the traction inverter system.

Considering that the active power consumed by the three resistors in Figure 3 was equal to the active power consumed by the resistor R_{d} in Figure 4, the power balance relationship shown in Equation (17) could be obtained.

$$3\left(\frac{I}{\sqrt{2}}\right)^2 R_e = \frac{u_{\mathrm{dc}}^2}{R_{\mathrm{d}}} \tag{17}$$

Thus, the expression of the equivalent resistance R_{d} could be obtained as follows:

$$R_{\mathrm{d}} = \frac{8\left[R_{\mathrm{e}}^2 + (\omega_{\mathrm{e}} L_{\mathrm{e}})^2\right]}{3m^2 R_{\mathrm{e}}} \tag{18}$$

According to the current relationship in Figure 4, ignoring the transient process of i_{dc}, the expression of the equivalent current source I_1 could be obtained as follows:

$$\begin{aligned} I_1 &= i_{\mathrm{dc}} - \tfrac{u_{\mathrm{dc}}}{R_{\mathrm{d}}} = \tfrac{3}{4} m I \cos\gamma - \tfrac{u_{\mathrm{dc}}}{R_{\mathrm{d}}} \\ &= \tfrac{3}{8} m^2 u_{\mathrm{dc}} \left[\sqrt{\tfrac{1}{R_{\mathrm{e}}^2 + (\omega_{\mathrm{e}} L_{\mathrm{e}})^2}} \cos\left[\arctan\left(\tfrac{\omega_{\mathrm{e}} L_{\mathrm{e}}}{R_{\mathrm{e}}}\right)\right] - \tfrac{R_e}{R_{\mathrm{e}}^2 + (\omega_{\mathrm{e}} L_{\mathrm{e}})^2} \right] \end{aligned} \tag{19}$$

2.3. Dq Impedance Modeling of Locomotives Considering Traction Inverter and Motor

This section establishes the dq impedance model of CRH5 and HXD_{2B} considering the inverter model and based on the rectifier model of the VGS [3,11,12]. As for the two types of vehicles, the main circuit structure of the traction drive units is the same, as shown in Figure 4, and the main circuit state equation of the converter could be written as:

$$\begin{cases} L_{\mathrm{n}} \frac{\mathrm{d}i_{\mathrm{n}}}{\mathrm{d}t} = e_{\mathrm{n}} - i_{\mathrm{n}} R_{\mathrm{n}} - d_n u_{\mathrm{dc}} \\ C_{\mathrm{d}} \frac{\mathrm{d}u_{\mathrm{dc}}}{\mathrm{d}t} = d_n i_{\mathrm{n}} - \left(\frac{u_{\mathrm{dc}}}{R_{\mathrm{d}}} + I_1\right) \end{cases} \tag{20}$$

In the above expression, when VD1 and VD4 are on while VD2 and VD3 are off, d_n is 1; when VD2 and VD3 are on while VD1 and VD4 are off, d_n is 0. To construct the dq impedance model, the state variable x needed to be decomposed into the dq axis through the inverse Park transformation. The relationship is shown in (21).

$$x_\alpha = x_d \cos\omega t - x_q \sin\omega t \tag{21}$$

Based on the conversion relationship of (21), ignoring the secondary power frequency ripple on the DC side, the state equation of the main circuit under the dq system was written as follows:

$$\begin{cases} L_{\mathrm{n}}\frac{\mathrm{d}i_d}{\mathrm{d}t} = e_d - R_{\mathrm{n}}i_d + \omega_1 L_{\mathrm{n}}i_q - d_d u_{\mathrm{dc}} \\ L_{\mathrm{n}}\frac{\mathrm{d}i_q}{\mathrm{d}t} = e_q - R_{\mathrm{n}}i_q - \omega_1 L_{\mathrm{n}}i_d - d_q u_{\mathrm{dc}} \\ C_{\mathrm{d}}\frac{\mathrm{d}u_{\mathrm{dc}}}{\mathrm{d}t} = \frac{1}{2}\left(d_d i_d + d_q i_q\right) - \left(\frac{u_{\mathrm{dc}}}{R_{\mathrm{d}}} + I_1\right) \end{cases} \tag{22}$$

By solving and analyzing the static operating point of the average model under the dq system, the values of the duty cycle, state variables, and output variables under steady-state conditions could be obtained. When the circuit is stable, the phase locked by the PLL is the same as the network voltage phase. At this time, the power factor is 1. Therefore, E_q and I_q are 0, and the steady-state values of the other variables are shown in (23).

$$\begin{cases} I_d = \frac{E_d - \sqrt{E_d^2 - 8R_{\mathrm{n}}U_{\mathrm{dc}}\left(\frac{U_{\mathrm{dc}}}{R_d} + I_1\right)}}{2R_{\mathrm{n}}} \\ D_d = \frac{E_d + \sqrt{E_d^2 - 8R_{\mathrm{n}}U_{\mathrm{dc}}\left(\frac{U_{\mathrm{dc}}}{R_d} + I_1\right)}}{2U_{\mathrm{dc}}} \\ D_q = \frac{-\omega_1 L_{\mathrm{n}}E_d + \omega_1 L_{\mathrm{n}}\sqrt{E_d^2 - 8R_{\mathrm{n}}U_{\mathrm{dc}}\left(\frac{U_{\mathrm{dc}}}{R_d} + I_1\right)}}{2R_{\mathrm{n}}U_{\mathrm{dc}}} \end{cases} \tag{23}$$

Equation (22) was expanded with a steady-state value and small signal at the static operating point [25]. Ignoring the steady-state component, we found that there are product terms for small signals, namely $\hat{d}_d\hat{u}_{dc}$, $\hat{d}_q\hat{u}_{dc}$, $\hat{d}_q\hat{i}_d$, and $\hat{d}_q\hat{i}_q$. The presence of these terms reflects the nonlinearity of the rectifier system. By ignoring these small-signal product terms, the system could be linearized to obtain the small-signal model of the system, as shown in Figure 5. The disturbance of the input voltage vector and the duty cycle vector were set to zero to derive the corresponding transfer function matrix. That is, the mathematical model of impedance under the dq system of the main circuit topology of CRH5 and $\mathrm{HXD_{2B}}$ was obtained as shown in (24).

$$\begin{cases} \boldsymbol{Z}_{RL} = \begin{bmatrix} R_{\mathrm{n}} + sL_{\mathrm{n}} & -\omega_1 L_{\mathrm{n}} \\ \omega_1 L_{\mathrm{n}} & R_{\mathrm{n}} + sL_{\mathrm{n}} \end{bmatrix} \boldsymbol{Z}_{RC} = \frac{R_{\mathrm{d}}}{sR_{\mathrm{d}}C_{\mathrm{d}}+1} \\ \boldsymbol{Z}_{\mathrm{in\_ol}} = \boldsymbol{Z}_{RL} + \frac{Z_{RC}}{2}\begin{bmatrix} D_d^{s2} & D_d^s D_q^s \\ D_d^s D_q^s & D_q^{s2} \end{bmatrix} \\ \boldsymbol{G}_{id} = -\boldsymbol{Z}_{\mathrm{in\_ol}}^{-1}\left(\frac{Z_{RC}}{2}\begin{bmatrix} D_d^s \\ D_q^s \end{bmatrix}\begin{bmatrix} I_d^s & I_q^s \end{bmatrix} + \begin{bmatrix} U_{\mathrm{dc}} & 0 \\ 0 & U_{\mathrm{dc}} \end{bmatrix}\right) \\ \boldsymbol{G}_{ue} = \frac{Z_{RC}}{2}\begin{bmatrix} D_d^s & D_q^s \end{bmatrix}\boldsymbol{Z}_{\mathrm{in\_ol}}^{-1} \\ \boldsymbol{G}_{ud} = \frac{Z_{RC}}{2}\begin{bmatrix} D_d^s & D_q^s \end{bmatrix}\boldsymbol{G}_{\mathrm{id}} \end{cases} \tag{24}$$

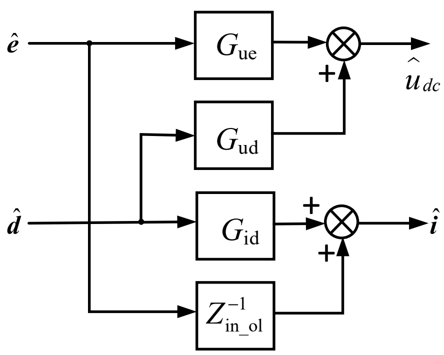

Figure 5. Small-signal matrix model of the main circuit.

As for HXD_{2B}, shown in Figure 2, since its control system introduces a feedforward amount $i_n^{ffd} = (\sqrt{2}i_{dc}u_{dc})/U_d$ to improve the dynamic response of the PI controller, when modeling considering the inverter, the steady-state value was written as $I_d^{ref} = \frac{\sqrt{2}U_{dc}^2}{U_d R_d} + \frac{\sqrt{2}U_{dc}I_1}{U_d}$. Under the conditions of unity power factor, the voltage loop has the following relationship:

$$\begin{cases} i_d^{ref} = i_n^{ref} = (K_{pvc} + \frac{K_{ivc}}{s})(u_{dc}^{ref} - u_{dc}) + \frac{\sqrt{2}i_{dc}u_{dc}}{U_d} \\ i_q^{ref} = 0 \end{cases} \tag{25}$$

By expanding (25) for small signals, (26) was obtained. The specific derivative process is shown in Appendix A.

$$\begin{bmatrix} \Delta i_d^{ref} \\ \Delta i_q^{ref} \end{bmatrix} = \begin{bmatrix} -(K_{pvc} + \frac{K_{ivc}}{s}) + \frac{2\sqrt{2}U_{dc}}{U_d R_d} + \frac{\sqrt{2}I_1}{U_d} & 0 \\ 0 & 0 \end{bmatrix} \begin{bmatrix} \Delta u_{dc} \\ 0 \end{bmatrix} \tag{26}$$

In order to verify the accuracy of the model, a train time-domain simulation model was built using the Matlab/Simulink platform, and the dq frequency sweep method based on Hilbert transformation was adopted to measure the impedance. Taking CRH5 as an example, the Bode curve of the impedance model considering the inverter was compared with the impedance measurement values, and the results are shown in Figure 6. The model impedance curve established in this paper was highly consistent with the impedance measurement points obtained by the time-domain simulation scan. This showed the effectiveness of the built model.

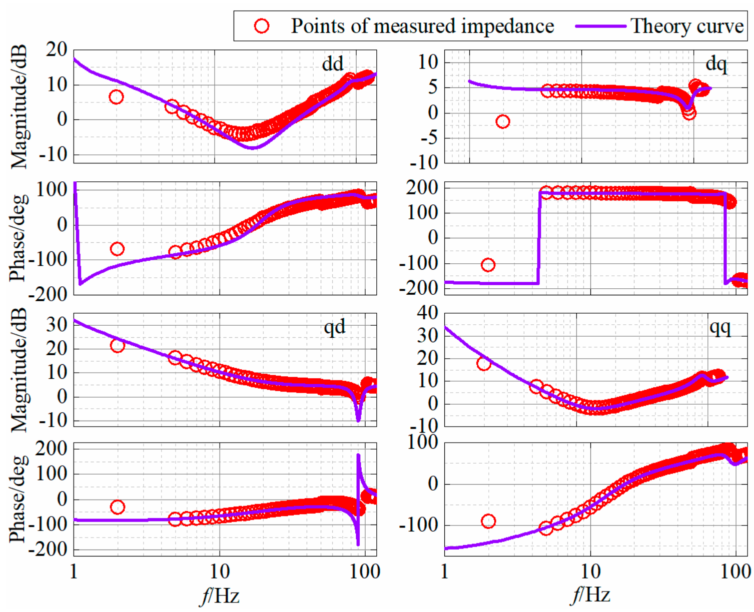

Figure 6. Comparison between the theoretical curve of dq impedance and measurement points of CRH5.

For a single train, several same-grid-side converters can be connected in parallel. For a CRH5 EMU, one power unit is a double rectifier, and there are five power units in total. Assuming that the onboard transformer of the EMUs works in the linear region, the impedance of the whole CRH5 EMUs could be converted to the model of the primary side:

$$\mathbf{Z}_{\mathbf{inCRH5}} = \frac{1}{5}\frac{\mathbf{Z}_{\mathbf{i}}|_{0.5C_{dc},\,2R_L}}{2k_{CRH5}^2} \tag{27}$$

where k_{CRH5} is the transformation ratio of the onboard transformer of the CRH5 EMUs, and k_{CRH5} = 1770/25,000.

The $\mathrm{HXD_{2B}}$ electric locomotive has six single rectifiers in parallel. Assuming the onboard transformer works in the linear region, the model for converting the impedance of the $\mathrm{HXD_{2B}}$ to the primary side is as follows:

$$\boldsymbol{Z}_{\mathbf{inHXD2B}} = \frac{1}{6}\frac{\boldsymbol{Z}_{\mathbf{i}}}{k_{\mathrm{HXD2B}}^{2}} \tag{28}$$

where k_{HXD2B} is the transformation ratio of the onboard transformer of the $\mathrm{HXD_{2B}}$ electric locomotive, and k_{HXD2B} = 2100/25,000.

2.4. Dq System Impedance Model of Mixed Passenger and Freight System

The passenger vehicle (CRH5) and the freight vehicle ($\mathrm{HXD_{2B}}$) run together in a mixed operation on the same arm, as shown in Figure 1. Although the two trains may be on the up and down lines, respectively, from the point of view of the electrical relationship, the impedances of the two are regarded as equivalent parallel connections [25]. If the number of CRH5 vehicles is a and the number of $\mathrm{HXD_{2B}}$ vehicles is b, the schematic diagram of the equivalent impedances of the whole VGS is shown in Figure 7.

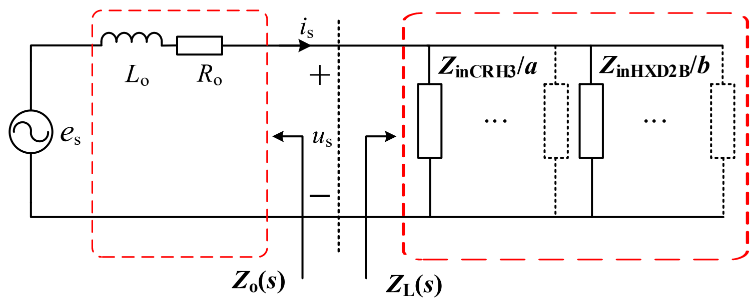

Figure 7. Schematic diagram of the equivalent impedances of the whole vehicle–grid coupling system.

It can be seen from Figure 7 that when two vehicles are connected in parallel, the overall impedance $\boldsymbol{Z}_{\mathbf{L}}$ of the load side in the VGS can be expressed as:

$$\boldsymbol{Z}_{\mathbf{L}} = \left(a(\boldsymbol{Z}_{\mathbf{inCRH5}})^{-1} + b(\boldsymbol{Z}_{\mathbf{inHDX2B}})^{-1}\right)^{-1} \tag{29}$$

3. Low-Frequency Oscillation Analysis of VGS with Mixed Passenger and Freight Locomotives

It can be seen from Figure 7 that if the equivalent impedance of the TN is defined as $\boldsymbol{Z}_{\mathbf{o}}(s)$, and the train-side impedance with the two types of vehicles connected in parallel is defined as $\boldsymbol{Z}_{\mathbf{L}}(s)$, the equivalent control diagram of the cascade system based on the impedance is as shown in Figure 5. Therefore, the system impedance return ratio matrix $L_{\mathrm{dq}}(s)$ is as follows (30) [12]:

$$\boldsymbol{L}_{\mathrm{dq}}(s) = \boldsymbol{Z}_{\mathbf{o}}(s)\boldsymbol{Z}_{\mathbf{L}}(s)^{-1} \tag{30}$$

It is evident from (30) that the system impedance return ratio matrix $\boldsymbol{L}_{\mathbf{dq}}$(s) is a transfer function matrix of 2 × 2, with two eigenvalues (λ_1(s) and λ_2(s)). It can be seen from the generalized Nyquist criterion that, on the premise that the source and load impedances are both stable (that is, neither $\boldsymbol{Z}_{\mathbf{o}}(s)$ nor $\boldsymbol{Z}_{\mathbf{L}}$(s) has a right-half-plane pole), the closed-loop system is stable if and only if the two eigenvalues λ_1(s) and λ_2(s) of $\boldsymbol{L}_{dq}$(s) do not enclose the (−1, j0) point.

We used eight different CRH5 and $\mathrm{HXD_{2B}}$ vehicles as simulation objects and built a simulation model in MATLAB/Simulink. The schematic diagram of the simulation structure is shown in Figure 8.

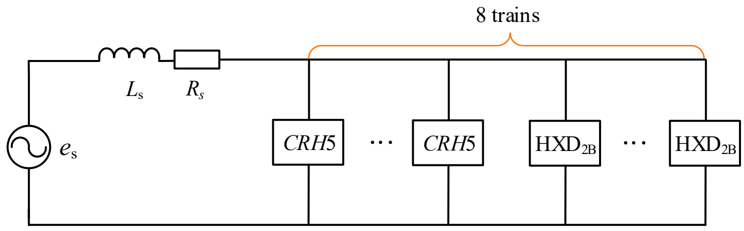

Figure 8. Schematic of the computer model built using Matlab/Simulink.

3.1. Analysis of the Influence of Different Proportions of Passenger and Freight Locomotives

The electrical stability analysis detailed in this section was mainly based on the mixed operation diagram shown in Figure 1. In order to visually show the influence of different train numbers on the system stability under mixed operation conditions, the trend of system stability changes was observed by altering the ratio of CRH5 trains and HXD_{2B} trains. In this section, mixed-operation configurations with a total of eight CRH5 and HXD_{2B} vehicles were analyzed, with the ratio of the two kinds of trains being changed. The generalized Nyquist curve and simulation of the system under three different passenger and freight mixed-operation ratios are shown in Figure 9. When other parameters in the system were unchanged, the intersection points of the Nyquist curve and the X-axis were -0.62, -0.82, and -1.01, respectively, when the ratio of CRH5 to HXD_{2B} was 5:3, 6:2, and 7:1. That is, as the proportion of CRH5 vehicles increased, the Nyquist curve gradually approached and surrounded $(-1, j0)$. When the mixing ratio was 7:1, a 2.8 H_Z oscillation occurred. The simulation results of eight CRH5 vehicles from reference [11,12] are shown in Figure 10. It can be seen that the system had an LFO of 2.5 Hz. The intersection point of the Nyquist curve and the X-axis was -1.91, which was greater than that in Figure 9. This indicates that the low-frequency stability of the system worsened.

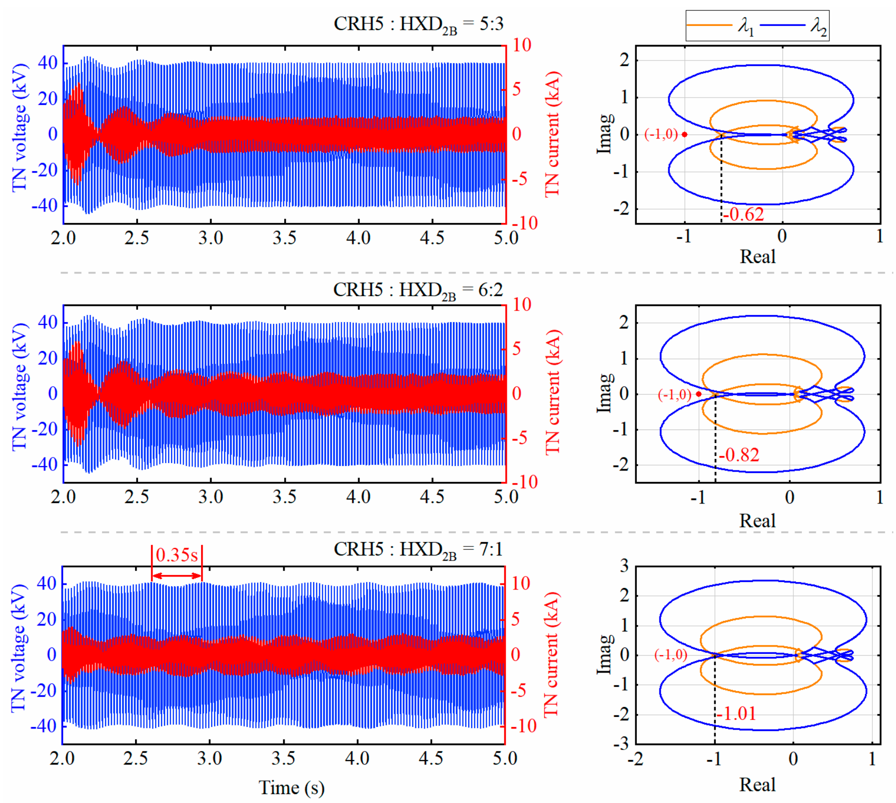

Figure 9. Simulation waveforms when the proportion of passenger and freight locomotives is changed.

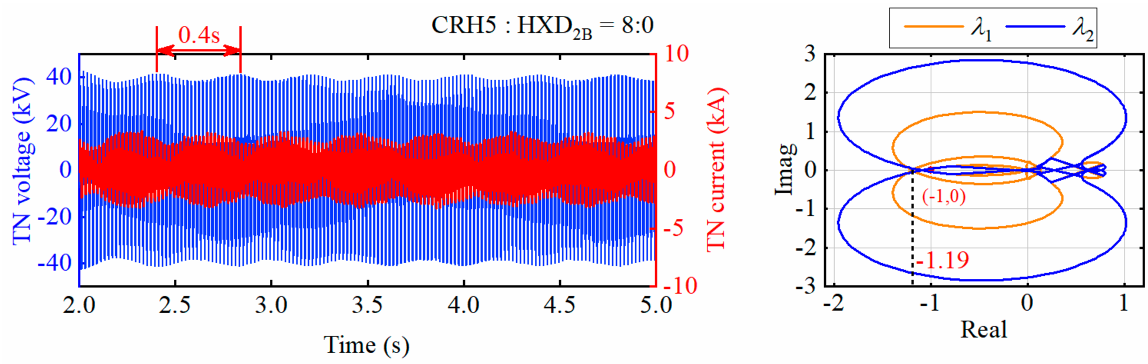

Figure 10. Simulation waveforms when the number of passenger locomotives is 8.

Therefore, we concluded that the greater the number of HXD_{2B} vehicles in the mixed VGS, the greater the stability margin of the whole system. Thus, avoiding a single train type will improve the stability of the system.

3.2. Analysis of the Influence of Different Control Parameters

Adjusting the train control parameters changes the impedance characteristics of the train and affects the system stability, so the LFO can be suppressed by adjusting these parameters [18].

When one HXD_{2B} and seven CRH5 were put into use, the proportional parameter Kpvc of the voltage loop of the CRH5 was reduced from 0.6 to 0.4. The intersection of the Nyquist curve and the X-axis changed from −1.01 to −0.8, and the system tended to be stable from the original 2.8 Hz oscillation. When the Kpvc was further reduced to 0.2, the intersection of the Nyquist curve and the X-axis became −0.74, and the system stability was further improved. The corresponding simulation results are shown in Figure 11, and the waveform tended to be stable. The simulation results were consistent with the theoretical analysis results, indicating that reducing the proportional gain of the voltage loop PI effectively improved the low-frequency stability of the VGS with mixed passenger and freight operation.

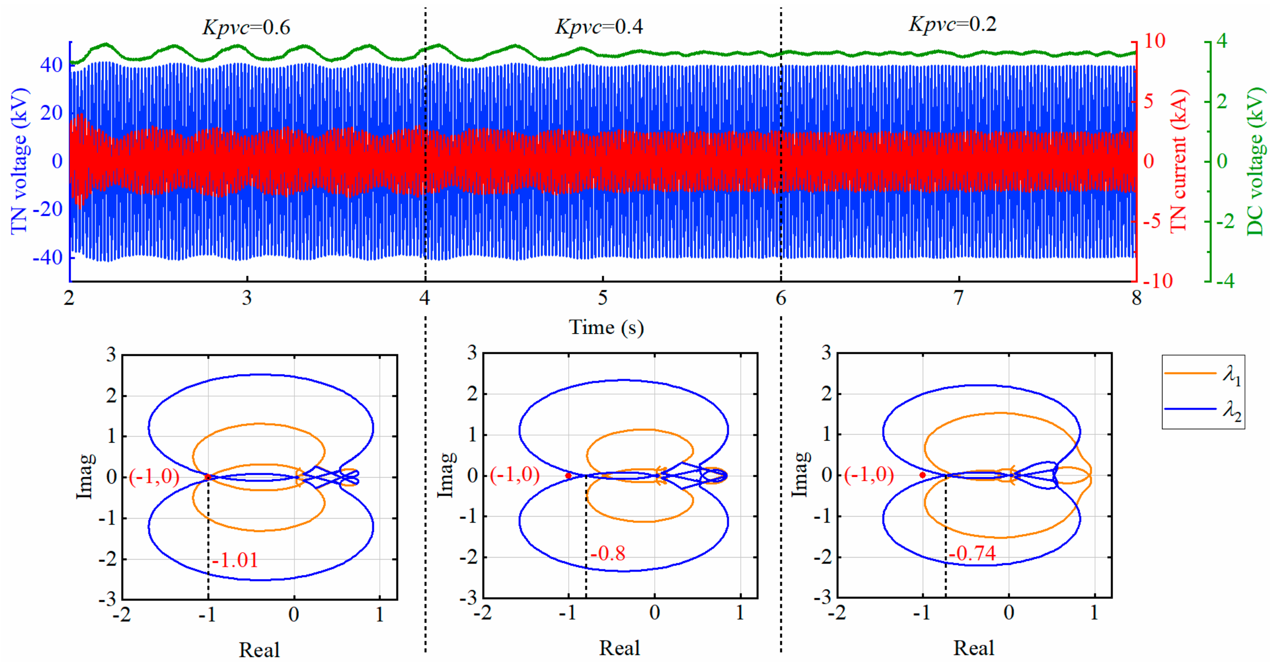

Figure 11. Influence of voltage loop PI proportional gain on system stability.

Similarly, the CRH5 train current loop proportional parameter Kpcc increased from 2 to 2.25. The intersection of the Nyquist curve and the X-axis changed from −1.01 to −0.84, and the system changed from experiencing 2.8 Hz oscillation to becoming stable. Further increasing the Kpcc to 2.7, the intersection of the Nyquist curve and the X-axis became −0.66, and the system stability was further improved. The corresponding simulation results are shown in Figure 12, and the waveform tended to be stable. The simulation results were consistent with the theoretical analysis results, indicating that increasing the proportional gain of the current loop PI effectively improved the low-frequency stability of the VGS with mixed passenger and freight operation.

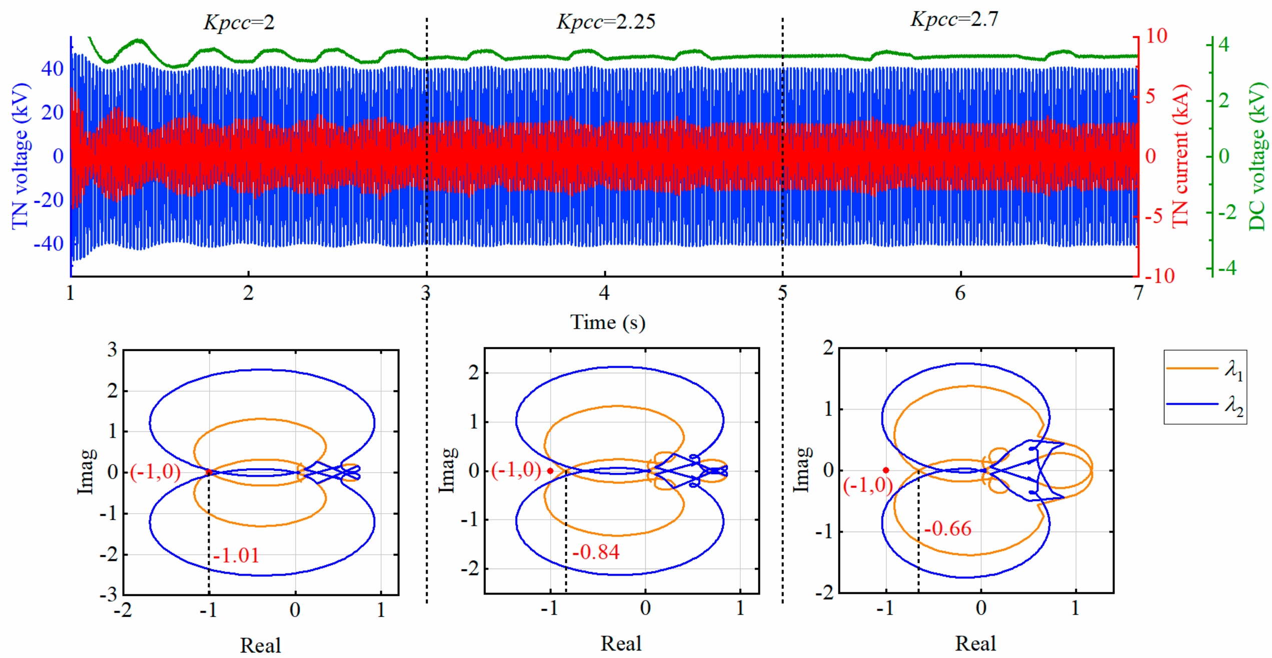

Figure 12. Influence of current loop PI proportional gain on system stability.

4. Low-Frequency Stability Conditions Analysis of VGS Based on Dominant Pole Theory

4.1. Frequency Analysis of VGS Based on Dominant Pole Theory

A block diagram of the VGS is shown in Figure 13. The VGS is actually a small-signal multi-variable closed-loop feedback system. The input signal is the voltage $\Delta e_s(s)$ on the high-voltage side of the on-board transformer, the output is the train's input current $\Delta i_s(s)$, and $Y_L(s)$ is the train's small-signal admittance model. Suppose there are trains of the same kind running on the line, and the small-signal admittance model is expressed as $Y_{in}(s)$. Then, $Y_L(s)$ can be expressed as $nY_{in}(s)$. For example, when the trains are all CRH5 EMUs, $Y_L(s)$ can be expressed as $nY_{inCRH5}(s)$. Similarly, when the trains are all HXD_{2B} electric locomotives, $Y_L(s)$ is expressed as $nY_{inHXD2B}(s)$. Therefore, the closed-loop transfer function matrix of the VGS in Figure 13 can also be expressed as follows:

$$\boldsymbol{H}_{\mathbf{ei}}(s) = \frac{\Delta i_s(s)}{\Delta e_s(s)} = \frac{n\boldsymbol{Y}_{\mathbf{in}}(s)}{\boldsymbol{I} + n\boldsymbol{Y}_{\mathbf{in}}(s) \cdot \boldsymbol{Z}_{\mathbf{o}}(s)} \tag{31}$$

For an MIMO system with a transfer function $\boldsymbol{H}_{\mathbf{ei}}(s)$, the poles and zeros can be obtained by solving the roots of the pole polynomial $p(s)$ and zero polynomial $z(s)$ equal to 0, respectively [18]. For the 2×2 square matrix analyzed in this paper, the zero-pole polynomial could be directly obtained as follows:

$$\frac{z(s)}{p(s)} = \det(\boldsymbol{H}_{\mathbf{ei}}) \tag{32}$$

To make the MIMO system stable, the following theorem can be referred to [18]:

$\boldsymbol{H}_{\mathbf{ei}}(s)$ is stable if and only if $\boldsymbol{H}_{\mathbf{ei}}(s)$ has no right-half-plane (RHP) poles.

When the above theorem is applied to the VGS, the stability conditions are as follows.

There is no RHP zero point in the switch transfer function matrix $\boldsymbol{G} = \boldsymbol{I} + nY_{\mathbf{in}}(\mathrm{s})\,\boldsymbol{Z}_{\mathbf{o}}(s)$ of the VGS.

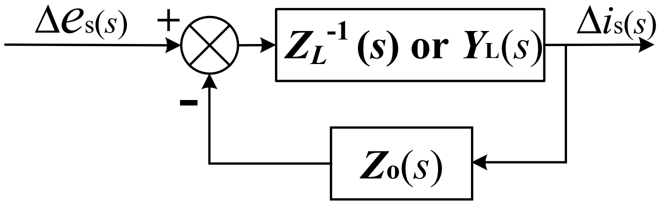

Figure 13. Block diagram of vehicle–grid cascade closed-loop system.

If the dominant pole is used to analyze the VGS, the pole of the CLTF must be calculated first. The CLTF poles are closest to the imaginary axis in the complex plane, and the pole whose distance is more than 10 times smaller than those of the other poles is the most likely to enter the right half plane and cause system instability. Therefore, the pair of poles that can easily cause system instability is called the dominant pole, since the zeros of the open-loop transfer function matrix correspond to the poles of the CLTF. Thus, in the VGS, in order to simplify the calculation process, the pole calculation can be converted into the zero calculation.

This pair of dominant poles can be expressed in the form of the damping ratio ζ and the natural oscillation angular frequency ω_{n}. In order to facilitate analysis together with the unit Hz of the oscillation frequency in the previous sections, the calculated dominant pole was reduced (divided by 2π), and the dominant pole was expressed as the damping ratio ζ and the expression of the natural oscillation frequency f_{n} in Hz, as shown in (33). In the following analysis, the dominant pole defined by the following formula was used to analyze the low-frequency stability of the VGS:

$$\begin{aligned} r_{1,2} &= -\xi f_{\mathrm{n}} \pm f_{\mathrm{n}}\sqrt{\xi^2 - 1} \\ &= -\xi f_{\mathrm{n}} \pm j f_{\mathrm{n}}\sqrt{1 - \xi^2} \end{aligned} \tag{33}$$

4.2. Low-Frequency Stability Conditions of VGS

In order to simplify the process of the low-frequency stability analysis in this section, we analyzed the traction power supply system of the CZ Railway from the perspective of power. First, it was assumed that only the reactance parameter X_{O} existed in the equivalent impedance of the grid side. All trains running on the line were thus equivalent to one load. Then, a schematic diagram of the simplified VGS, as shown in Figure 14, could be obtained.

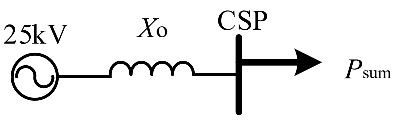

Figure 14. Simplified schematic diagram of VGS.

The SCR in the power system was defined as the reciprocal of the power reactance X_{O} per unit value. In the vehicle–grid cascade system, the per-unit voltage reference value (U) was 25 kV. The power reference value took the rated capacity (S) of two single-phase traction stations as 60 MVA, and the SCR could be expressed as follows:

$$\mathrm{SCR} = \frac{1}{X_O/X} = \frac{1}{X_O/\left(\frac{U^2}{S}\right)} = \frac{U^2}{SX_O} = \frac{25^2}{60 \times 2X_O} \tag{34}$$

The authors of [18] mentioned that when the damping ratio corresponding to the dominant pole is in the 10^{-3} order of magnitude, the system has the possibility of entering a critically stable or even unstable state. In the following analysis, the standard of the damping ratio corresponding to the dominant pole was greater than 0.01, and it was determined that the VGS could ensure the low-frequency stable state. Therefore, in the following work, for different ratios of CRH5 EMUs and HXD_{2B} electric locomotives, we adjusted the power supply reactance X_O, so that the damping ratio corresponding to the dominant pole was only greater than 0.01 when the two types of trains were running alone. Then, this was substituted into (34) to calculate the minimum stable SCR when the VGS remained stable.

According to the above theory of dominant poles and SCR, the relationship between the number of trains and the minimum SCR was obtained as shown in Figure 15.

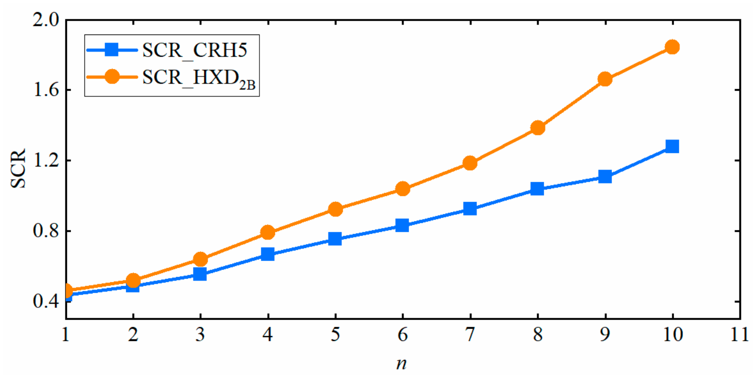

Figure 15. The relationship curve between the number of trains n and SCR.

It can be seen from Figure 15 that there was a linear relationship between the minimum stable SCR and the number of vehicles of the two types of trains. The fitting results for the relationship are shown in (35).

$$\begin{cases} \text{SCR\_CRH5} = 0.0582n + 0.3784 & (n \geq 1) \\ \text{SCR\_HXD}_{\text{2B}} = 0.1712n + 0.2896 & (n \geq 1) \end{cases} \tag{35}$$

When the SCR had a value in the area above the straight line, the VGS remained stable. If the SCR was converted into the short-circuit capacity S_{SC}, and the number of running trains n was converted into the sum P_{sum} of the rated power of all trains, the linear proportional coefficient μ of the two could be defined as shown in (36). (The rated power of the CRH5 vehicles is 5.5 MW, and the rated power of the HXD_{2B} vehicles is 9.6 MW).

$$\begin{cases} \mu_{\text{CRH5}} = \dfrac{\Delta S_{\text{SC}}}{\Delta P_{\text{sum}}} = \dfrac{S}{P_{CRH5}} \dfrac{\Delta \text{SCR\_CRH5}}{\Delta n} = \dfrac{120}{5.5} \dfrac{\Delta \text{SCR\_CRH5}}{\Delta n} \\ \mu_{\text{HXD2B}} = \dfrac{\Delta S_{\text{SC}}}{\Delta P_{\text{sum}}} = \dfrac{S}{P_{\text{HXD2B}}} \dfrac{\Delta \text{SCR\_CRH5}}{\Delta n} = \dfrac{120}{9.6} \dfrac{\Delta \text{SCR\_HXD}_{\text{2B}}}{\Delta n} \end{cases} \tag{36}$$

In Figure 15, the slope of the straight line representing the CRH5 EMU was converted to a ratio of ΔS_{SC} to ΔP_{sum} equal to 1.27, while the slope of the straight line representing the HXD_{2B} was 2.14. For the VGS composed of CRH5 EMUs and the TN, when $\mu_{\text{CRH5}} \geq 1.27$, the VGS was in a stable state, and there was no low-frequency oscillation. When $\mu_{\text{CRH5}} < 1.27$, the VGS may have experienced LFO or even lost stability. For the VGS composed of HXD_{2B}, when $\mu_{\text{HXD2B}} \geq 2.14$, the VGS was in a stable state, and there was no low-frequency oscillation. When $\mu_{\text{HXD2B}} < 2.14$, the VGS may have experienced LFO or even lost stability. From the above analysis, the following conclusions could be drawn: for any kind of running train, there is always a critical μ_0, and when $\mu \geq \mu_0$, the vehicle–grid cascade system can ensure its low-frequency stability. For the passenger and freight mixed-car network system formed by the CRH5 EMUs and the HXD_{2B} electric locomotives studied in this paper, when $\mu \geq 2.14$, the vehicle-network cascade system can maintain low-frequency stability.

4.3. Simulation Verification

In order to verify the accuracy of the two curves obtained in Figure 15, a simulation model was built using the MATLAB/Simulink platform, and simulation analysis was carried out for $n = 1$ and 5. When only one CRH5 EMU was connected, according to the relationship curve between the number of CRH5 vehicles and the minimum stable SCR in Figure 15, the minimum stable SCR of the vehicle network system was 0.437, the X_O was 11.93 Ω, and the maximum value of the grid-side inductance L_O was 38 mH. Therefore, in the simulation, when R_O was set to 3.6 Ω and L_O was set to 40 mH, the grid-side current and voltage waveforms were obtained as shown in Figure 16. A low-frequency oscillation of 3 Hz occurred in the VGS at this time.

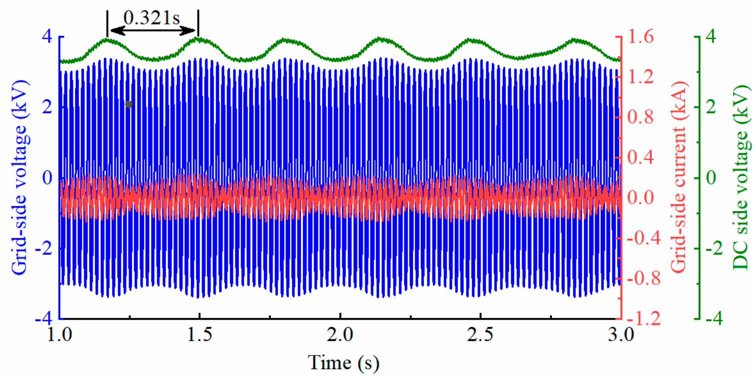

Figure 16. Grid-side voltage and current waveforms when a single CRH5 vehicle was connected.

In the same way, when only one HXD_{2B} electric locomotive was connected, according to the relationship curve between the number of HXD_{2B} vehicles and the minimum stable SCR in Figure 15, the minimum stable SCR value was 0.461, the X_O was 11.3 Ω, and the maximum value of the grid-side reactance L_O was 36 mH. Therefore, in the simulation, when R_O was set to 3.6 Ω and L_O was set to 37 mH, the grid-side current and voltage waveforms were obtained as shown in Figure 17. A low-frequency oscillation of 3.5 Hz occurred in the VGS at this time.

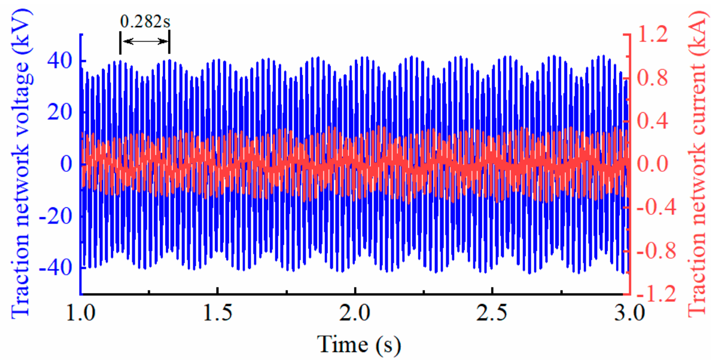

Figure 17. Grid-side voltage and current waveforms when a single HXD_{2B} vehicle was connected.

When five CRH5 EMUs were connected at the same time, according to the relationship curve in Figure 15, the minimum stable SCR value was 0.754, the X_O was 6.9 Ω, and the maximum value of the grid-side reactance L_O was 22 mH. Therefore, in the simulation, when R_O was set to 2.2 Ω and L_O was set to 25 mH, the grid-side current and voltage waveforms were as shown in Figure 18. A low-frequency oscillation of 3 Hz occurred in the VGS at this time.

When five HXD_{2B} EMUs were connected at the same time, according to the relationship curve in Figure 15, the minimum stable SCR value was 0.922, the X_O was 5.65 Ω, and the maximum value of the grid-side reactance L_O was 18 mH. Therefore, in the simulation, when R_O was set to 2.2 Ω and L_O was set to 19 mH, the grid-side current and voltage waveforms were obtained as shown in Figure 19. A low-frequency oscillation of 6.3 Hz occurred in the VGS at this time.

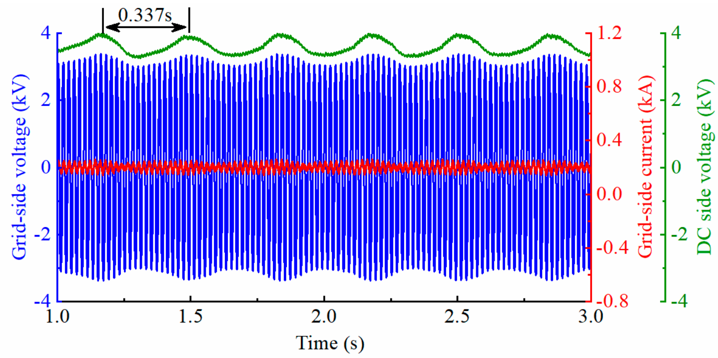

Figure 18. Grid-side voltage and current waveforms when five CRH5s are connected.

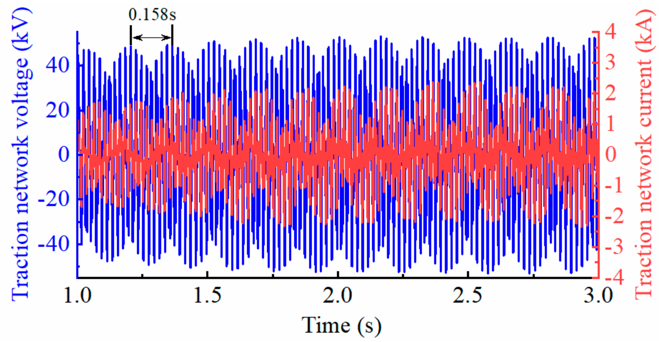

Figure 19. The voltage and current waveforms on the grid side when five HXD2Bs vehicles were connected.

Due to the performance of the simulation equipment, only the simulation waveforms for the connection of a single train and five trains (Figures 16–19) are provided, which verify the validity of the curve obtained in Figure 15. Therefore, in order to keep the VGS stable, the impedance of the TN and the train scheduling method must be designed according to the curve requirements provided in Figure 15.

The above steps can also be followed for other types of trains running on the railway., The dominant pole of the CLTF matrix of the VGS is obtained according to the type and number of locomotives, followed by the value of the maximum power source reactance X_O under critical conditions. Then, the minimum stable SCR value is calculated by Equation (34), the relevant curve is obtained, and the TN is designed to reduce the possibility of LFO.

5. Conclusions

In this paper, a small-signal impedance model of a multi-vehicle mixed-operation VGS considering the traction inverter system was established. The influence of different passenger/cargo locomotive ratios and different locomotive control parameters on the LFO was analyzed. In addition, using the dominant pole theory to analyze the low-frequency stability conditions of the VGS, the relationship between the number of mixed trains and the minimum short-circuit ratio of the system was obtained. Finally, the accuracy of the model built by the simulation experiment and the correctness of the theoretical analysis were verified, and the following conclusions were drawn.

(1) The measurement results of Figure 6 show the correctness of our established equivalent model of the traction inverter system. Therefore, it provides a theoretical basis for the selection of the DC-side load of the rectifier.
(2) The low-frequency oscillation analysis results of the VGS under the mixed operation of passenger and freight trains showed that an increase in the number of HXD_{2B} vehicles

reduces the low-frequency oscillations. Therefore, compared with the operating conditions of a single locomotive, the mixed operation system with multiple types of locomotives is more stable.

(3) According to the analysis results of the LFO under the dominant pole theory, in order to keep the system stable, it is necessary to design the train scheduling according to the relationship between the SCR and the number of locomotives based on (35).

Author Contributions: Data curation, Y.W. and T.L.; Investigation, J.L., F.L. and Y.S.; Methodology, Q.Z., W.Z. and Z.L. All authors have read and agreed to the published version of the manuscript.

Funding: This research was funded by the Science and Technology Project of the State Grid Sichuan Electric Power Company (SGSCJY00GHJS2200025).

Data Availability Statement: All the data has been provided in the paper.

Conflicts of Interest: The authors declare no conflict of interest.

Nomenclature

Abbreviation	Meaning
EMUs	Electric multiple units
LFO	Low-frequency oscillation
CRH	China Railway High-speed
HXD	He xie dianli
DQDC	D-q decoupling control
TDCC	Transient direct current control
SOGI	Second-order generalized integrator
PLL	Phase-locked loop
TN	Traction network
RHP	Right half plane
$\mathrm{E_d}$	D-axis steady voltage
$\mathrm{f_1}$	Fundamental frequency
$\mathrm{f_p}$	Disturbance frequency range
$\mathrm{R_n}$	Equivalent resistance of secondary side of vehicle transformer
$\mathrm{L_n}$	Equivalent inductance of secondary side of vehicle transformer
$\mathrm{C_d}$	DC-side support capacitor
$\mathrm{U_d}$	Steady DC-link voltage
$\mathrm{f_s}$	Switch frequency
VGS	Vehicle–grid system
R_d	DC-side equivalent resistance
d_n	Duty cycle of upper bridge arm switch
ω_1	Fundamental angular frequency
R_s	Grid-side equivalent resistance
L_s	Grid-side equivalent inductance
i_dc	DC-side current
I_1	Equivalent current source
e_n	TN voltage
i_n	Rectifier current
SCR	Short-circuit ratio
$\mathrm{K_{uSOGI}}$	Voltage SOGI module ratio
$\mathrm{K_{iSOGI}}$	Current SOGI module ratio
$\mathrm{K_{Ppll}}$	Proportionality coefficient of PLL
$\mathrm{K_{Ipll}}$	Integral coefficient of PLL
$\mathrm{K_{Pi}}$	Proportionality coefficient of current loop
$\mathrm{K_{Ii}}$	Integral coefficient of current loop
$\mathrm{K_{Pu}}$	Proportionality coefficient of voltage loop
$\mathrm{K_{Iu}}$	Integral coefficient of voltage loop
CLTF	Closed-loop transfer function

Appendix A

Under the conditions of a unity power factor, the voltage loop has the relationship based on (25).

According to Figure 4, on the DC-side resistance branch,

$$i_{dc} = I_1 + \frac{u_{dc}}{R_d} \tag{A1}$$

Substituting (A1) into (25), we obtained

$$i_d^{ref} = (K_{pvc} + \frac{K_{ivc}}{s})(u_{dc}^{ref} - u_{dc}) + \frac{\sqrt{2}u_{dc}(\frac{u_{dc}}{R_d} + I_1)}{U_d} \tag{A2}$$

Expanding the above formula for small signals produced the following:

$$u_{dc} = U_{dc} + \Delta u_{dc} \tag{A3}$$

Substituting (A3) into (25), we obtained

$$\begin{aligned} i_d^{ref} &= (K_{pvc} + \tfrac{K_{ivc}}{s})(u_{dc}^{ref} - (U_{dc} + \Delta u_{dc})) \\ &+ \tfrac{\sqrt{2}U_{dc}^2 + 2\sqrt{2}U_{dc}\Delta u_{dc} + \sqrt{2}\Delta u_{dc}^2}{R_d U_d} + \tfrac{\sqrt{2}I_1}{U_d}\Delta u_{dc} \end{aligned} \tag{A4}$$

Ignoring the steady-state component and the small-signal product term Δu_{dc}^2, the system could be linearized, and the following relationship was finally obtained:

$$\Delta i_d^{ref} = (-(K_{pvc} + \frac{K_{ivc}}{s}) + \frac{2\sqrt{2}U_{dc}}{R_d U_d} + \frac{\sqrt{2}I_1}{U_d})\Delta u_{dc} \tag{A5}$$

Translating this into matrix form, Equation (26) was obtained.

References

1. Menth, S.; Markus, M. Low frequency power oscillations. *Electr. Railw. Syst.* **2006**, *104*, 216–221.
2. Danielsen, S.; Molinas, M.; Toftevaag, T.; Fosso, O.B. Constant power load characteristic's influence on the low-frequency interaction between advanced electrical rail vehicle and railway traction power supply with rotary converters. In Proceedings of the Modern Electric Traction (MET), Gdańsk, Poland, 24–26 September 2009; pp. 1–6.
3. Kong, R.; Lv, X.; Wang, X.; Chang, M.; Ge, M. Modeling and Analysis of Low Frequency Oscillation in Train-Network System under Mixed Operation of Trains. In Proceedings of the CSEE 2022, Lisbon, Portugal, 10–12 April 2022; pp. 2315–2324.
4. Zhou, Y.; Hu, H.; Yang, X.; Yang, J.; He, Z.; Gao, S. Analysis of Low-frequency Oscillation in Train-TN Coupling System of Electrified Railway. *Proc. CSEE* **2017**, *37*, 72–80.
5. Wu, S.; Liu, Z. Low-Frequency Stability Analysis of VGS with Active Power Filter Based on dq-Frame Impedance. *IEEE Trans. Power Electron.* **2021**, *36*, 9027–9040. [CrossRef]
6. Hu, H.T.; Tao, H.D.; Wang, X.F.; He, Z.; Gao, S. Train–Network Interactions and Stability Evaluation in High-Speed Railways–Part I: Phenomena and Modeling. *IEEE Trans. Power Electron.* **2018**, *33*, 4627–4642. [CrossRef]
7. Hu, H.; Tao, H.; Wang, X.; Blaabjerg, F.; He, Z.; Gao, S. Train–Network Interactions and Stability Evaluation in High-Speed Railways—Part II: Influential Factors and Verifications. *IEEE Trans. Power Electron.* **2018**, *33*, 4643–4659. [CrossRef]
8. Wu, S.; Jatskevich, J.; Liu, Z.; Lu, B. Admittance Decomposition for Assessment of APF and STATCOM Impact on the Low-Frequency Stability of Railway VGSs. *IEEE Trans. Power Electron.* **2022**, *37*, 15425–15441. [CrossRef]
9. Hu, H.; Zhou, Y.; Li, X.; Lei, K. Low-Frequency Oscillation in Electric Railway Depot: A Comprehensive Review. *IEEE Trans. Power Electron.* **2021**, *36*, 295–314. [CrossRef]
10. Liu, Z.; Zhang, G.; Liao, Y. Stability research of high-speed railway EMUs and TN cascade system considering impedance matching. *IEEE Trans. Ind. Appl.* **2016**, *52*, 4315–4326. [CrossRef]
11. Liao, Y.; Liu, Z.; Zhang, H.; Wen, B. Low-frequency stability analysis of single-phase system with dq-frame impedance approach—Part I: Impedance modeling and verification. *IEEE Trans. Ind. Appl.* **2018**, *54*, 4999–5011. [CrossRef]
12. Liao, Y.; Liu, Z.; Zhang, H.; Wen, B. Low-frequency stability analysis of single-phase system with DQ-frame impedance approach—Part II: Stability and frequency analysis. *IEEE Trans. Ind. Appl.* **2018**, *54*, 5012–5024. [CrossRef]
13. Mollerstedt, E.; Bernhardsson, B. Out of Control Because of Harmonics-An Analysis of the Harmonic Response of an Inverter Locomotive. *IEEE Control Syst. Mag.* **2000**, *20*, 70–81.

14. Yue, X.; Wang, X.; Blaabjerg, F. Review of Small-Signal Modeling Methods Including Frequency-Coupling Dynamics of Power Converters. *IEEE Trans. Power Electron.* **2019**, *34*, 3313–3328. [CrossRef]
15. Jiang, X.; Hu, H.; Yang, X.; He, Z.; Qian, Q.; Tricoli, P. Analysis and Adaptive Mitigation Scheme of Low Frequency Oscillations in AC Railway Traction Power Systems. *IEEE Trans. Transp. Electrif.* **2019**, *5*, 715–726. [CrossRef]
16. Lv, X.; Wang, X.; Che, Y.; Li, L. Dynamic phasor modelling and low-frequency oscillation analysis of the single-phase VGS. *CSEE J. Power Energy Syst.* 2020; *Early Access*.
17. Liao, Y.; Wang, X. Impedance-based stability analysis for interconnected converter systems with open-loop RHP poles. *IEEE Trans. Power Electron.* **2020**, *35*, 4388–4397. [CrossRef]
18. Wang, H.; Wu, M.; Sun, J. Analysis of Low-Frequency Oscillation in Electric Railways Based on Small-Signal Modeling of VGS in dq Frame. *IEEE Trans. Power Electron.* **2015**, *30*, 5318–5330. [CrossRef]
19. Yang, W.; Jin, J.; Song, E. Analysis and suppression of current harmonic in harbin-dalian TN for mixed passenger and freight traffic. *World Invert.* **2016**, *2*, 47–51.
20. Wang, H.; Tian, M.; Sun, L.; Zhou, G. Simulation study on harmonic characteristics of AC-DC locomotive mixed running TN. *Railw. Stand. Des.* **2020**, *64*, 165–169.
21. Feng, X. *Electric Traction AC Drive and Its Control System*; Higher Education Press: Beijing, China, 2009; pp. 78–154.
22. Zhang, Q.; Zhang, Y.; Huang, K.; Tasiu, I.A.; Lu, B.; Meng, X.; Liu, Z.; Sun, W. Modeling of Regenerative Braking Energy for Electric Multiple Units Passing Long Downhill Section. *IEEE Trans. Transp. Electrif.* **2022**, *8*, 3742–3758. [CrossRef]
23. Wang, H.; Han, Z.; Liu, Z.; Wu, Y. Deep Reinforcement Learning Based Active Pantograph Control Strategy in High-Speed Railway. *IEEE Trans. Veh. Technol.* **2022**. [CrossRef]
24. Zhang, J.; Li, H.; Feng, X. Research on load equivalent model of four-quadrant converters. *Trans. China Electrotech. Soc.* **2008**, *23*, 72–76.
25. Liu, H.; Xie, X.; Liu, W. An Oscillatory Stability Criterion Based on the Unified dq-Frame Impedance Network Model for Power Systems with High-Penetration Renewables. *IEEE Trans. Power Syst.* **2018**, *33*, 3472–3485. [CrossRef]